Onset of erosion and avalanche for an inclined granular bed sheared by a continuous laminar flow

Thomas Loiseleux[a)]
Laboratoire Fluides Automatique et Systèmes Thermiques (FAST), Universités Paris 6, 11 and CNRS (UMR7608), Bât. 502, 91405 Orsay Cedex, France and Groupe Dynamique des Fluides et Acoustique, Unité de Mécanique, Ecole Nationale Supérieure de Techniques Avancées (ENSTA), 32 Bd Victor, 75015 Paris, France

Philippe Gondret, Marc Rabaud, and Delphine Doppler
Laboratoire Fluides Automatique et Systèmes Thermiques (FAST), Universités Paris 6, 11 and CNRS (UMR7608), Bât. 502, 91405 Orsay Cedex, France

(Received 21 December 2004; accepted 15 September 2005; published online 19 October 2005)

The transport inception of immersed grains is studied experimentally with *laminar* flow conditions in a Hele-Shaw cell when varying the tilt angle of the cell and the water flow rate. Varying these two parameters, grains are either motionless, rolling on the bed surface, or avalanching downwards. This paper focuses on the determination of the onset for grain motion either by erosion or by avalanche. For a horizontal interface, onset for erosion corresponds to a constant critical Shields number $\theta_c = 0.14$ at small particle Reynolds number ($\mathrm{Re}_d < 1$) but decreases as Re_d^{-1} at larger particle Reynolds number ($\mathrm{Re}_d > 1$). For tilted bed, the onset of erosion increases when the flow is opposed to gravity. Both results are compared to a standard model based on a balance of the forces acting on a single grain lying on a tilted plane. When tilt angles are large, avalanches occur. The maximum angle of stability is modified by the flow and increases slightly when the flow acts against gravity. This behavior is compared to a continuous model where a few layers of grains are about to slide. © *2005 American Institute of Physics*. [DOI: 10.1063/1.2109747]

I. INTRODUCTION

The understanding of many natural phenomena—river bedforms, for instance—or industrial processes such as oil production or underwater infrastructure positioning, requires a thorough knowledge of granular transport mechanisms and particularly of motion inception. However, even if the notions of erosion and avalanche may be intuitively captured, a physical description remains a difficult task.

In most submarine areas or in rivers, sediment transport is dominated by *erosion*, meaning by a sand flux induced by a fluid flow. Depending on the contact frequency of moving grains with the granular bed, this mechanism is divided into bed load if particles are rolling, sliding or hopping and suspended load if they are dragged far from the sand/fluid interface by the current. For laminar flows or weak bottom shear stress, bed load is the only active mode.[1,2] Since the first attempt by du Boys[3] in 1879 to model this transport mechanism, various studies aimed at relating the sediment bed load flux to the flow characteristics. Whether empirical such as Meyer-Peter and Muller,[4] mechanistic[5,6] or based on a sheet flow approach,[7] these widely used models all give an estimation of the sand flux as a function of the excess shear stress $(\tau - \tau_c)$, where τ is the bottom tangential shear stress, and τ_c its critical value below which all grains are at rest and above which transport occurs. Hence, bed load transport modeling relies on a good description of this critical shear τ_c. However, despite many efforts for almost seventy years, the mechanism of incipient erosion is still not satisfactorily captured. Shields[8] introduced the representation of the critical nondimensional shear stress θ_c, which expresses the ratio between the bottom shear stress and the apparent weight of a bead, as a function of the turbulent Reynolds number Re_* based on the grain diameter d, fluid kinematic viscosity $\nu = \eta/\rho$, and friction velocity $u_* = \sqrt{\tau_c/\rho}$. Since this pioneering work, many studies on the inception of erosion have been conducted.[9] In such a representation, a general trend is observed, but collected data exhibit a large scattering. This scatter may partially come from the chosen criterion as stated by Van Rijn,[10] Cheng *et al.*,[11] or Lavelle and Mofjeld[12] but also from the nature—turbulent or laminar—of the flow as underlined by White.[13] Indeed, for a turbulent flow, velocity fluctuations strongly modify the instantaneous shear stress imposed to grains at a sand bed surface. Granular transport may then be observed for small mean values of the shear and quantitative results are then highly dependent on the turbulent intensity of the flow. Various experimental works have been devoted to erosion onset determination with viscous liquids, such as White,[13] White,[14] Mantz,[15] Yalin and Karahan[16], or Pilotti and Menduni,[17] in order to keep low values of particle Reynolds number. All these studies have been conducted in linear flumes, from 1 to 10 m long, with small diameter silicate, quartz, or glass particles sheared by oil, water, glycerin, or a glucose-water solution. Considering the flow Reynolds number, only few studies correspond to laminar flows with no free surface interactions,[13,16] and their results confirm White's assumption:[13] the critical Shields numbers for laminar flows effectively appear to be larger

a)Electronic mail: thomas.loiseleux@ensta.fr

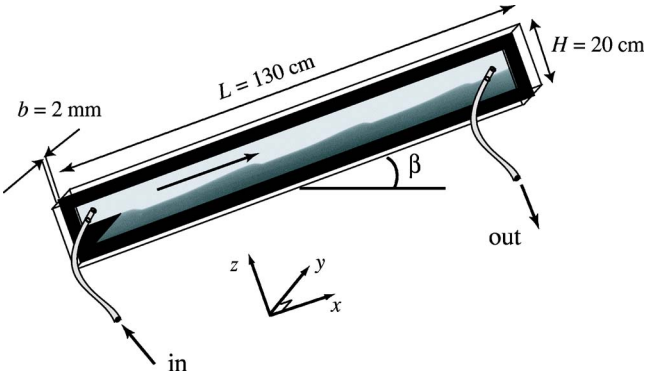

FIG. 1. Sketch of the experimental flume that can be tilted by an angle β in the cell plane.

than those classically found for turbulent flows. Nevertheless, collected data are still scattered and no model reproduces the observed trend. This may be explained by the multiple possible definitions for motion threshold. This problem has recently been evidenced by Charru *et al.*[18] who carefully looked at individual particle motion in a very well-controlled laminar experiment, i.e., a viscous Couette flow in an annular geometry.

Few studies have been devoted to the effect of a bed slope on erosion threshold.[1,19–21] The essential result is the observation of a decrease (respectively, increase) of the critical Shields number measured for down sloping (respectively up sloping) beds, relatively to its value for a horizontal bed.

Concerning avalanches, many studies have been conducted these last years about the loss of stability of a dry granular slope above a critical angle of *avalanche* β_c.[22] However, very few studies exist on steep underwater slopes,[23–25] and none are concerned with the effect of a hydrodynamic surface flow, whether uphill or downhill, on β_c. Nevertheless, this situation is often encountered in nature, on the continental shelf slope for instance, or on the lee side of dunes.[26]

In the present article, we focus on the effect of a slope on erosion threshold and the effect of a fluid flow on granular avalanche onset. In order to gain in physical understanding of the mechanisms, our experimental setup is very simplified as described in Sec. II: spherical glass beads, weak size polydispersity, unidirectional laminar flow, analytical expression of the flow velocity profile, constant shear all along the bed, etc. Our measurements for erosion and avalanche thresholds are presented in Sec. III for various grain sizes and compared to adequate models in Sec. IV. Finally, the main conclusions are summarized in Sec. V.

II. EXPERIMENTAL SETUP

The threshold of granular transport is studied under continuous flow in a Hele-Shaw cell. This cell consists of two glass plates of length $L=130$ cm and height $H=20$ cm separated by a small gap $b=2$ mm (Fig. 1).

The cell is partially filled with sieved glass beads (~ 10 cm), of mean diameter d and density $\rho_s=2.5\times 10^3$ kg/m^3. Five different diameters $d=90$, 110, 140, 180, and 220 μm with a rather narrow size dispersion ($\pm 10\%$) have mainly been studied. The number of beads in the cell gap b/d remains thus in the range $9<b/d<22$, which ensures that intergrain friction remains dominant with respect to grain-wall friction.[27] The beads are fully immersed in water (density $\rho_l=10^3$ kg/m^3 and viscosity $\eta=10^{-3}$ Pa s at the temperature $T=20\,^\circ$C). As we focus on the coupling between a hydrodynamic continuous flow and the granular bed surface, there is no air in the cell in order to avoid possible interactions with free surface waves. The in-loop hydraulic circuit is composed of the Hele-Shaw cell, a decanting tank, a filter, a centrifugal pump withdrawing the liquid and a calibrated flowmeter. By adjusting the pump frequency, a flow rate Q is imposed through the cell in the range $0\leqslant Q\leqslant 2.5$ l/min. In order to study the effect of the bed slope on the erosion process the cell can rotate in the vertical plane parallel to the two glass plates. The tilt angle, denoted β, between the horizontal and the cell longitudinal axis can be modified continuously in the range $[-60^\circ,+60^\circ]$ and is measured by a digital inclinometer with a resolution of $\pm 0.1^\circ$. Water flows from left to right and by convention β is chosen positive when water flows uphill and negative when it flows downhill, the horizontal situation corresponding to $\beta=0$. The possibility of tilting the cell up to large angles is used to trigger a sequence of large avalanches in both directions before each experiment to recover an initial flat interface. Our two experimental control parameters are then the flow rate Q and the tilt angle β. The glass plates allow for an easy visualization of the motion of grains. Movies are obtained by charge coupled device cameras fixed to the cell and rotating with it. In such a narrow flume, as far as the flow remains laminar, the velocity profile of the water current is parabolic across the gap b. The gap averaged velocity $\bar{U}$ is thus constant except near the upper wall or close to the granular surface. If we neglect the fact that the bed is rough at the grain scale and that the bed is porous which means that velocity is not exactly zero at the bed surface as shown by Beavers and Joseph,[28] this mean velocity $\bar{U}$ goes exponentially to zero at the bed surface with a characteristic length scale equal to the cell thickness b.[29] The shear close to the interface then writes $\dot{\gamma}\approx 3.26\bar{U}/b$ (see the Appendix). These results are valid as long as the flow remains laminar in the cell, i.e., as long as the flow Reynolds number $\mathrm{Re}_b=\rho_l\bar{U}b/\eta$, based on the mean fluid velocity $\bar{U}$ and the cell gap size b, remains below 900.[30] This is the case in the present study as $\mathrm{Re}_b<500$. However even if this Reynolds number is important for determining if the bulk flow is laminar or turbulent, it is not the relevant parameter at the grain scale. More appropriate is the particle Reynolds number $\mathrm{Re}_d=\rho_l u_0 d/\eta$ based on the grain diameter d and on the typical velocity u_0 of the fluid at the center of a grain lying on the granular surface. As the grain diameter d is much smaller than the scale b of evolution of the velocity profile, we estimate the typical velocity u_0 at the height $d/2$ over the bed as $u_0=\dot{\gamma}d/2$. In practice, the mean water velocity $\bar{U}$, and finally $\dot{\gamma}$ and u_0 are deduced from the flow rate Q and the height of flowing water ($H_w\sim 10$ cm). For water flowing typically at $\bar{U}=20$ cm/s, $\mathrm{Re}_b=400$ and $\mathrm{Re}_d=5.3$ for 180 μm beads. These values show that the water flow above the interface remains laminar and that the wake of an individual motion-

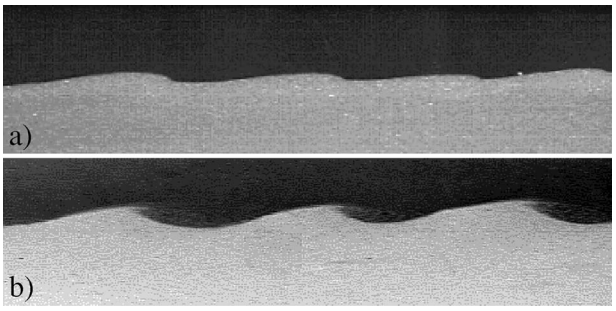

FIG. 2. Bedforms observed on 15 cm of the granular surface ($d=180\ \mu$m) with water flowing from left to right. (a) Triangular ripples propagating to the right on a flat interface ($\beta=0$, $\theta=0.25$). The asymmetry between the upstream and downstream slopes is clearly visible. (b) Vortex ripples propagating to the right on a tilted interface ($\beta=+45°$, $\theta=0.25$). The vortices behind the crest are clearly visible (note that the image has been rotated to recover apparent horizontality).

less grain is transitional but still time independent with a drag coefficient C_D of the order of 5 typically.

In the literature concerned with erosion process the classical dimensionless number used to describe the onset is the Shields number.[8] This parameter is the ratio between tangential and normal stresses acting on a grain and may then be written as

$$\theta = \frac{\eta\dot{\gamma}}{\Delta\rho g d}, \tag{1}$$

where $\Delta\rho=\rho_s-\rho_l$ (indices s and l stand for solid and liquid). Note that this Shields number is defined for a horizontal interface ($\beta=0$) and the effect of the tilt angle on the critical Shields number is one of the aims of this article.

III. ONSET OF GRAIN TRANSPORT BY EROSION OR AVALANCHE

In this article we mainly focus on the onset of grain motion, however we first describe qualitatively what occurs at and above onset.

A. Qualitative results

Let us consider first the case of a horizontal granular interface ($\beta=0$). At low flow rate the grains are motionless. For a larger flow rate some grains move from time to time but eventually stop definitively and it is only for a slightly larger flow rate Q_c that at any time few grains are rolling on the bed, possibly stopping but starting again soon. Still increasing the flow rate the rolling grains increase in number and move faster. After some time (typically few minutes) the interface is no more flat but some regularly spaced ripples are observed all along the cell [Fig. 2(a)]. These ripples propagate in the stream-wise direction and grow in amplitude and in wavelength during their motion all along the cell. When the ripples are well formed, grains roll along the upstream slope of each ripple and fall in avalanche on their lee face. We call these structures *triangular ripples*. This general description of erosion process remains true when the cell is tilted by a small positive or negative angle, except that the onset of erosion is continuously modified as described in Sec. III B.

With zero flow rate and now increasing slowly the tilt angle, the bed is first motionless. An avalanche starts when the pile reaches its maximum angle of stability $\beta_0\sim\pm30°$. As the cell is long and filled with a liquid, the avalanche lasts for long even if the angle is not increased anymore. Indeed the fluid may strongly affect the duration of avalanches.[25] At onset the avalanche only concerns the few upper grain layers. Increasing further the tilt angle makes the avalanche stronger, i.e., the number of moving layers increases and the grains move faster, as observed in dry grains experiments.[22] Doing the same experiment with a fixed small water flow (downwards or upwards) and increasing the tilt angle, the general description remains valid but the critical avalanche angle β_c becomes flow-rate dependent. It is only for large tilt angles and large uphill flow ($\theta>0$ and $\beta>0$) that dynamical structures are observed at the interface. This case corresponds to a competition between avalanche that tends to move the grains downwards and the water flow that tends to transport them upwards. These structures grow spatially and propagate in the stream direction [Fig. 2(b)]. When they become large enough, a strong vortex is observed downstream each crest. These *vortex ripples* are generated by an instability between the water stream and the avalanche stream flowing undertow, analogous to the Kelvin-Helmholtz instability at the interface between two fluid layers flowing at different velocities. Similar mechanism is observed during sedimentation of particles in tilted tubes limiting the Boycott effect.[31] Detailed description of the observed structures and of their dynamics will be the subject of a future publication.

In the following we will restrict ourselves to the onsets of grain motion by erosion or avalanche processes by varying both the tilt angle and the water flow rate. We present first quantitative results for the grain diameter $d=180\ \mu$m (Sec. III B) before comparing with other grain diameters (Sec. III C).

B. Quantitative results for $d=180\ \mu$m

As already stated in the introduction, the determination of the onset of erosion Q_c is not an easy or obvious task. Indeed the existence of transient erosion state below Q_c, that depends on the bed configuration, is known for long and has been recently described in details by Charru *et al.*,[18] Cheng *et al.*,[11] or Lavelle and Mofjed.[12] In front of this difficulty, we choose a definition of the onset based on our observation for slowly increasing water flow rate. This corresponds to the "visual method" described in the review article of Buffington and Montgomery.[32] We watch carefully to grain motion on a 10 cm long part of the granular bed, using a video CCD situated approximately in the middle of the cell. At low flow rates, grains are motionless. Then, for intermediary flow rates some beads are intermittently extracted from the bed surface, but this slight intermittent transport may end after few minutes. We chose to define the erosion threshold Q_c as the lowest flow rate for which grains are still being eroded after fifteen minutes. Note that with our criterion, even just above threshold, the particle flow may be intermittent as no

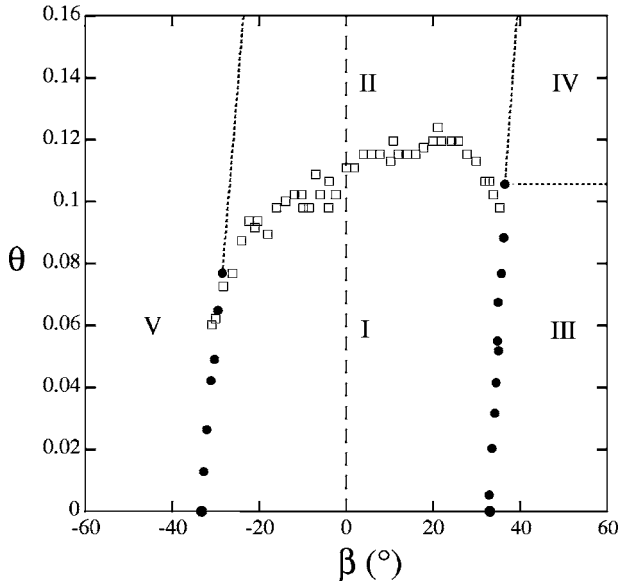

FIG. 3. Onset of erosion $\theta_c(\beta)$ (□) and of avalanche $\beta_c(\theta)$ (●) in the plane of parameters (θ,β) for glass beads of diameter $d=180$ μm. Domains I–V are described in the text. Dotted lines corresponds to approximate boundaries between domains.

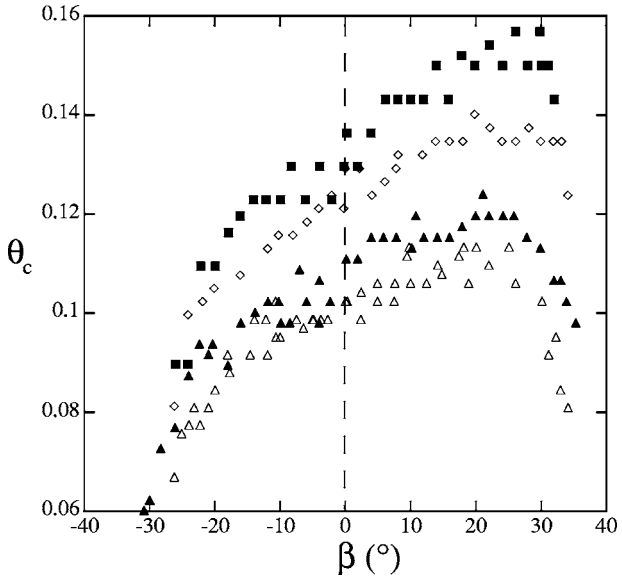

FIG. 4. Critical Shields number for erosion as a function of the cell angle for various grain diameters: (■) $d=110$ μm, (◇) $d=140$ μm, (▲) $d=180$ μm, and (△) $d=220$ μm.

grain may move at a given instant, but transport will rapidly start again and after some times a ripple pattern develops at the sand/fluid interface. For the grain diameter $d=180\pm10$ μm and $\beta=0°$ we found the critical flow rate $Q_c=32.5\pm2.5$ cm^3/s ($\overline{U_c}=17.5$ cm/s) for the onset of erosion. This value corresponds to the critical particle Reynolds number $\mathrm{Re}_{d_c}=4.6$ and to the Shields number $\theta_c=0.108$.

The critical angle for which an avalanche starts is easier to determine. A close inspection reveals that just above the angle of maximum stability, few layers of beads (typically 2 or 3) are flowing downwards. This *collective* behavior clearly differs from the erosion case where only few *individual* grains are rolling downstream over a motionless bed. For the $d=180$ μm glass beads the angle at which an avalanche starts without any water flow is $\beta_0=\pm32°$. This value is slightly larger than the usual value for a 3D pile but can be explained by the stabilizing effect of the confinement due to the close lateral walls. Indeed Courrech *et al.*[27] have shown that for a number of beads in the gap given by the ratio $b/d\approx11$, the maximum angle of stability is increased by a few degrees with respect to the angle that would be observed for large cells.

For an inclined cell, the influence of the tilt angle β on the onset of erosion θ_c and of the flow rate θ on the onset of avalanche β_c is presented in Fig. 3. Each data point corresponds to the average of several realizations. The data points separate the parameter space in a region (labeled I) where no grain motion is observed from other domains where erosion and/or avalanche are observed. In region II, only erosion is observed for small positive or negative tilt angles ($-30°<\beta<+30°$) and triangular ripples similar to those presented in Fig. 2(a) slowly appear. In region III only downward avalanches are observed even if the flow would tend to move the grains upward. In region IV both downward avalanche and uphill surface erosion are observed. These two counter effects rapidly give birth to vortex ripples such as presented in Fig. 2(b). Finally in region V both erosion and avalanche tend to move the grains downwards and it is therefore difficult to determine which process is dominant. In Fig. 3 only positive flow rates are presented but the results are symmetrical via the transformation $(\theta,\beta)\rightarrow(-\theta,-\beta)$.

The effect of tilting the cell is logically to increase the onset of erosion for positive slope and to decrease it for negative slope. Although this effect is almost linear with the tilt angle between $-20°<\beta<+20°$ it presents a maximum for $\beta\approx+20°$, as if, when β becomes closer to the avalanche angle β_c, surface grains were easier to force out. The same destabilizing effect is also observed for $\beta<-20°$ when gravity acts in the flow direction. In both cases this weakening effect appears clearly before the slope reaches the natural avalanche angle β_0.

To study the effect of the flow rate on the avalanche angle we first impose a flow rate and then tilt slowly the cell until an avalanche starts. We thus determine the maximum angle of stability of the pile at the corresponding water flow rate. For each flow rate two values corresponding to positive and negative angles are obtained, leading to the boundaries between the domain I and the domains III or V of Fig. 3. Note that using the symmetry these points corresponds to a continuous evolution of β_c from negative to positive θ values. This dependence is almost linear with a large coefficient as a large flow rate is necessary to increase the avalanche angle by only a few degrees.

C. Effect of the grain diameter

Similar experiments have been done for grain diameters in the range 90 $\mu\mathrm{m}\leqslant d\leqslant220$ μm. The results for the onset of erosion are presented in Fig. 4. This figure shows that the data follow the same trend but do not collapse on a master curve when using the Shields number θ. This means that

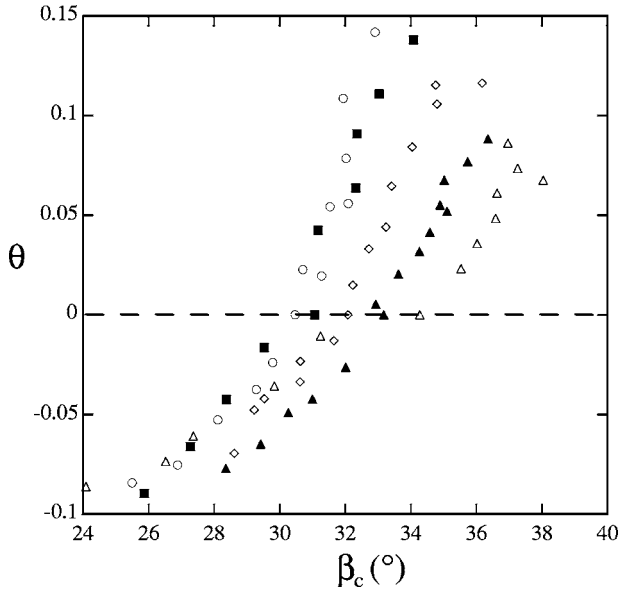

FIG. 5. Avalanche angles observed for different flow rate, presented in the plane (θ,β) for: (○) $d=90$ μm, (■) $d=110$ μm, (◇) $d=140$ μm, (▲) $d=180$ μm, and (△) $d=220$ μm. Negative Shields numbers correspond to downhill flows.

even the erosion threshold on a horizontal bed does not correspond to a unique θ value. Indeed, dimensional analysis shows that bed erosion is not only a function of the Shields number but also of a second dimensionless number, for example Re_d.[5] We will elaborate on this point in the next section.

Figure 5 presents the results for avalanche critical angles with water flow. The data are presented here on a single plot for positive or negative values of the Shields number θ. The data evolution for a given diameter is continuous but the gradient seems slightly different for positive or negative values of θ: downhill flows seem slightly more efficient to modify the angle of avalanche than uphill flows. Again the data do not collapse on a single curve, mainly because the natural avalanche angle (without water flow), β_0, increases with the bead diameter, probably due to an increasing arching effect between the lateral walls.[27]

IV. GRAIN TRANSPORT MODELING

We now attempt to model the effect of the bed slope on erosion threshold as well as the effect of water flow on the avalanche onset by a description of the forces acting on the granular material.

A. Erosion model

A balance of the forces acting on a single static bead located on a plane and submitted to a flow is most probably the simplest model that may be used for understanding the onset of erosion. This idea is sustained by the experimental observation that, at erosion onset, beads move individually. Many authors[10,13,21] developed this simplified approach. In the following, we will present an adaptation of this idea to our specific situation.

Four forces govern the grain equilibrium: its apparent weight F_W, a fluid drag force F_D, a normal force F_N and a solid friction force $F_f=\mu_e F_N$. For a static grain just about to move, the balance of forces along the bed in the direction of the flow writes

$$-\frac{\pi d^3}{6}\Delta\rho g\sin\beta-\mu_e\frac{\pi d^3}{6}\Delta\rho g\cos\beta+\alpha 3\pi\eta d u_0\Phi(\mathrm{Re}_d)=0. \tag{2}$$

The first term is the apparent weight of the grain and the second corresponds to the maximum value of the static friction, described by a Coulombic force. A friction angle δ may be defined based on the apparent friction coefficient $\mu_e=\tan\delta$, which takes into account the solid friction but also the roughness and the traps of the surface which is experimentally not flat due to the presence of the supporting beads underneath. In the following we will assume μ_e and thus δ as constant for all the grain diameters. The third term stands for the fluid drag force F_D. As the particle Reynolds number is relatively small we write the drag force as $F_D=\alpha 3\pi\eta d u_0\Phi(\mathrm{Re}_d)$, where $3\pi\eta d u_0$ stands for the Stokes force acting on a motionless sphere in an homogeneous and infinite flow of velocity u_0 at very low Re_d. The factor α is a constant that takes into account the particular geometry and more precisely the fact that the grain is close to a surface and moreover a rough one. The factor α has been theoretically evaluated by O'Neill[33] and King and Leighton.[34] They obtained $\alpha\approx 1.70$ for a smooth or rough sphere on a flat plane submitted to a constant shear rate. The function $\Phi(\mathrm{Re}_d)$ is a correction factor to the Stokes drag when the Reynolds number is not small: it tends toward 1 for vanishing Re_d and toward $C_D\mathrm{Re}_d/24$ (with a corresponding drag coefficient $C_D\approx 0,4$) when $\mathrm{Re}_d\to\infty$. For $\mathrm{Re}_d<1000$, a good fit for $\Phi(\mathrm{Re}_d)$ is the empirical law[35]

$$\Phi(\mathrm{Re}_d)=1+0.15\mathrm{Re}_d^{0.687}. \tag{3}$$

If θ_0 and Re_{d0} denote respectively the Shields number and the particle Reynolds number at onset for a horizontal bed $\beta=0$. Then, from Eq. (2), the critical Shields number θ_c for all β for grain motion may be expressed as

$$\frac{\theta_c}{\theta_0}=\frac{\Phi(\mathrm{Re}_{d0})}{\Phi(\mathrm{Re}_d)}\frac{\sin(\beta+\delta)}{\sin\delta}, \tag{4}$$

with

$$\theta_0=\theta_c(\beta=0)=\frac{\tan\delta}{9\alpha\Phi(\mathrm{Re}_{d0})}. \tag{5}$$

This onset value θ_c is then a function of the slope of the bed β, of the friction angle δ and of the particle Reynolds number Re_d. Note that this model is valid for positive or negative β as F_f remains in both cases opposite to F_D. Similar equation has been already obtained by previous authors[1,2,20,36] with a two-dimensional analysis based on the fluid forces or torques acting on a single grain laying on two beads.

Let us now compare this result to the experimental onset of erosion obtained for a horizontal or tilted cell.

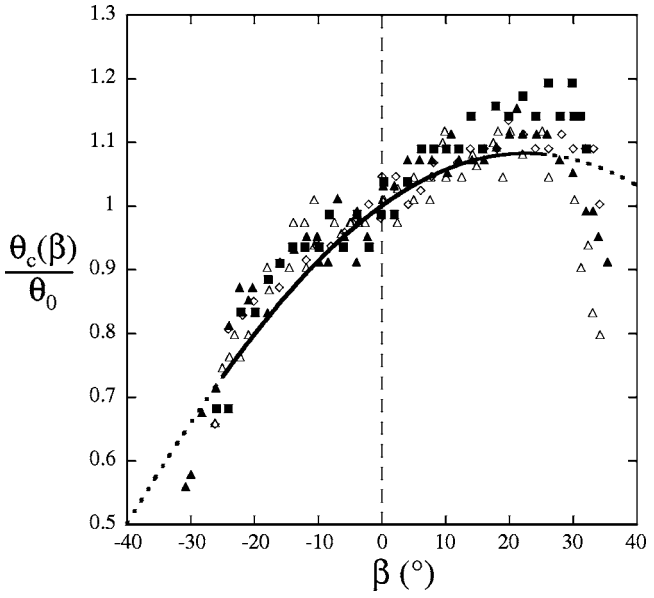

FIG. 6. Evolution of the experimental ratio θ/θ_0 of the erosion onset as a function of the slope angle for various grain diameters: (■) $d=110$ μm, (◇) $d=140$ μm, (▲) $d=180$ μm, and (△) $d=220$ μm. The plain curve corresponds to Eq. (4) adjusted in the range $[-25°, 25°]$ with friction angle $\delta=67.5°$ (—).

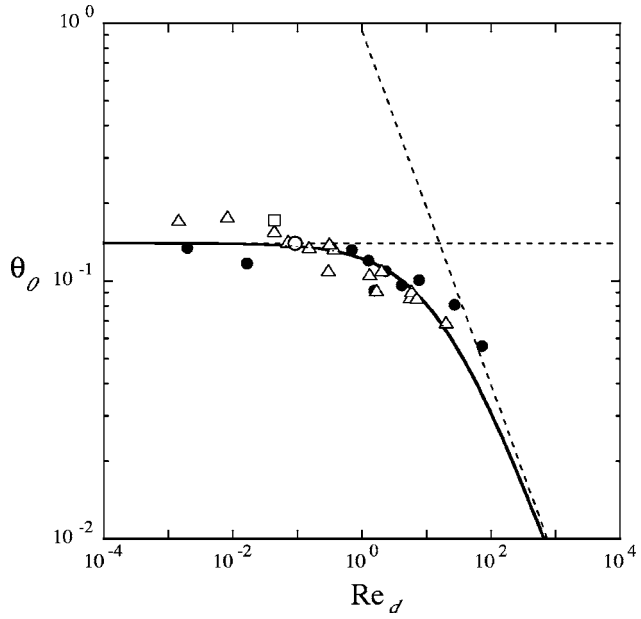

FIG. 7. Critical Shields number θ_0 for laminar erosion on a horizontal bed ($\beta=0°$) as a function of the particle Reynolds number Re_d. Continuous line corresponds to Eq. (5) with fitting coefficient $\alpha=1.95$, dashed line to the corresponding asymptotic behavior at small and large Re_d and data points to our results (●) and those of White (Ref. 13) (□), Yalin and Karahan (Ref. 16) (△), Mouilleron-Arnould (Ref. 37) (○).

When renormalized by θ_0, the corresponding experimental data of Fig. 4 collapse on a master curve as evidenced by Fig. 6. The comparison between the prediction given by Eq. (4) is satisfactory for $|\beta| \leqslant 25°$ but fails to catch the strong decrease of the critical Shields number observed for higher slopes ($|\beta| \geqslant 25°$). The best fit is obtained for $\delta=67.5° \pm 3.5°$. This value is large compared to the natural angle of avalanche β_0 but is, however, in agreement with previous experimental results of White[13] giving also a similar large value of $\delta\,(55°)$.

The variation of θ_0 is presented as a function of Re_{d0} in Fig. 7, using Eq. (3) for $\Phi(\mathrm{Re}_d)$ and the fitting value $\alpha=1.95\pm0.35$, together with the two asymptotic behaviors $\Phi(\mathrm{Re}_d)=1$ and $\Phi(\mathrm{Re}_d)\approx \mathrm{Re}_d/60$ corresponding to small and large particle Reynolds numbers. Our results for horizontal interface and various grain diameters (data from Fig. 4 with $\beta=0$) are plotted as well as other points corresponding to larger grains diameter $d=130$, 360, and 570 μm. Data corresponding to the two smaller values of critical Reynolds number are achieved for particles of diameter $d=110$ μm immersed in two different water-glycerine mixtures, respectively, 57% and 72% glycerine in mass. (The density of each glycerol-water mixture was measured with a digital densimeter and the viscosity was inferred from tables: for the 57% mixture, $\rho=1145$ kg/m^3, $\eta=8.8\times10^{-3}$ Pa s and for the 72% mixture, $\rho=1188$ kg/m^3, $\eta=27\times10^{-3}$ Pa s at $T=20$ °C.) Results deduced from previous studies found in the literature for the onset of erosion in the restricted cases of laminar flows with no free-surface interactions are also displayed.[13,16,37]

The agreement between the model and the data is quite good for the fitting value $\alpha=1.95\pm0.35$ which is close to the value $\alpha\approx1.7$ calculated by O'Neill[33] for the drag coefficient of a sphere near a smooth plane. Note that these values of the critical Shields corresponding to laminar flow are significantly larger than the one corresponding to turbulent flows (see, e.g., Fig. 5 of the article by Yalin and Karahan[16]). In the limit of low particle Reynolds number ($\mathrm{Re}_d<1$), the laminar flow Shields number for the onset of erosion is constant and equal to $\theta_c=0.14$. For large particle Reynolds numbers ($\mathrm{Re}_d>1$), θ_c decreases as Re_d^{-1}.

Note that adding a lift force induced by the flow on the grain, following the work of Leighton and co-workers[34,38] does not change significantly the model as long as we remain in their domain of validity ($\mathrm{Re}_d \ll 1$) or even if we extend it to particle Reynolds numbers of order 1.

B. Avalanche model

Grain motion during avalanches appears experimentally different from erosion motion. During avalanches, we do not observe the motion of individual grains but the collective downward motion of several layers of beads. For modeling the avalanche process, we thus consider now a layer of width b, length L and thickness h which is just about to move as a whole in a downhill avalanche parallel to the granular surface tilted by the critical angle β_c (Fig. 8). The equilibrium equation tangential to the pile can be written as

$$-c\Delta\rho ghLb\sin\beta_c-\mu_a c\Delta\rho ghLb\cos\beta_c+\tau bL-\Delta Pbh=0. \tag{6}$$

The first term is the apparent weight F_W of the layer having the solid volume fraction c. The second term is the uphill (opposed to the downhill avalanche motion) solid friction force F_f between the bottom of the layer and the motionless pile with the effective friction coefficient μ_a. (Note

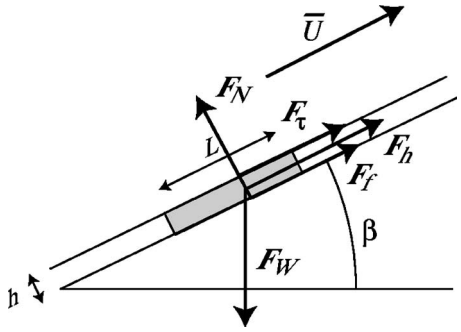

FIG. 8. Sketch of the forces acting on a small volume of grains close to the interface, when an uphill flow is present.

that this effective friction coefficient is different from the friction coefficient μ_e in the erosion inception model.) The third term corresponds to the tangential fluid friction force $F_\tau = \tau bL$ on the bed surface with the tangential stress $\tau = \eta\dot{\gamma} \approx 3.26\eta\bar{U}/b$. Depending on the flow direction, this force can be uphill ($U>0$) or downhill ($U<0$). The fourth and last term corresponds to a pressure force $F_h = \Delta P bh$ acting inside the bed in the direction of the flow. Indeed, a longitudinal pressure gradient $\Delta P/L = -12\eta\bar{U}/b^2$ exists along the cell equilibrating viscous fluid force (Darcy law in a Hele-Shaw cell). Note that as the pressure gradient is the same in the whole cell, the water flow in the bed is typically 10^{-6} times smaller than the flow outside the bed. Again depending on the flow direction, this last pressure force can be uphill ($\Delta P<0$, $U>0$) or downhill ($\Delta P>0$, $U<0$).

When introducing the Shields number and the avalanche angle for zero flow rate $\beta_0[\beta_0 = \tan^{-1}(\mu_a)]$, Eq. (6) reduces to

$$\theta = c\frac{b}{d}\left(\frac{b}{h}+\frac{12}{3.26}\right)^{-1}\frac{\sin(\beta_c-\beta_0)}{\cos\beta_0}. \tag{7}$$

As $\beta_c - \beta_0$ remains experimentally small, Eq. (7) may be written as

$$\beta_c \approx \beta_0 + \theta\cos\beta_0\frac{1}{c}\frac{d}{b}\left(\frac{b}{h}+\frac{12}{3.26}\right). \tag{8}$$

This model predicts that for a given diameter the critical angle β_c evolves almost linearly with the Shields number θ, with coefficients depending on d as suggested by Fig. 5.

To test this model, the experimental data of Fig. 5 are plotted in Fig. 9 as $\theta\cos\beta_0 d/b$ as a function of $\beta_c - \beta_0$, using the experimental values of β_0 measured for each diameter. Data exhibit a good agreement with the model, even if the decrease of the avalanche angle in the case of downhill flows appears stronger than the corresponding increase for uphill flows. The best fit for all the data of Fig. 5 by Eq. (7) with a packing fraction value $c=0.6$ usually assumed for a granular bed gives $h=560$ μm for the thickness of the avalanche. This value is compatible with the observed avalanche thickness at threshold which is of the order of half a millimeter and does not seem to vary significantly with the grain diameter. This last result is in agreement with the work of Courrech du Pont *et al.*[27] Indeed, they observed that for beads smaller than 400 μm, the avalanche thickness at threshold does not depend anymore on the grain size. Note

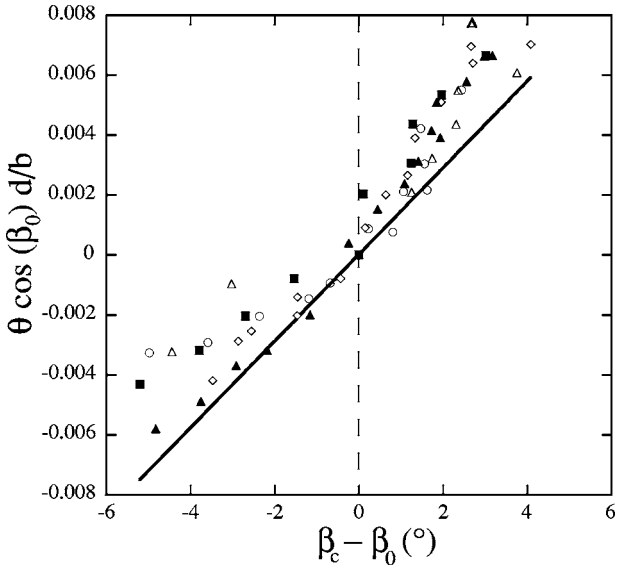

FIG. 9. Evolution of $\theta\cos\beta_0 d/b$ as a function of the difference of slopes $\beta_c - \beta_0$ for various grain diameters [(○) $d=90$ μm, (■) $d=110$ μm, (◇) $d=140$ μm, (▲) $d=180$ μm, and (△) $d=220$ μm] and fit by Eq. (7) for $c=0.6$ and $h=560$ μm.

that the value determined for h shows that the flow force F_h inside the bed has to be taken into account as it is of the same magnitude as the surface shear force F_τ: $F_\tau/F_h = 3.26b/12h \approx 1$.

The evolution of the avalanche angle without flow β_0 on the particle diameter d is displayed in Fig. 10. Experimental data compare well with a linear fit taking into account the friction wall effects $\tan\beta_0 = \tan\beta_0^\infty + Nd/b$, as proposed by Courrech du Pont,[39] where $\beta_0^\infty = 27.3°$ is the angle without wall effects and $N=1.1$.

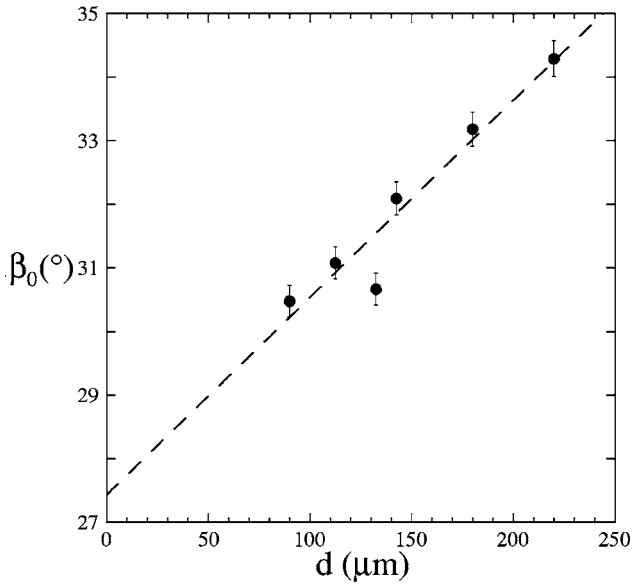

FIG. 10. Experimental evolution of the angle of avalanche obtained without water flow for increasing particle diameter and fit (---) by $\tan\beta_0 = \tan\beta_0^\infty + Nd/b$ with $\beta_0^\infty = 27.3°$ and $N=1.1$.

V. CONCLUSION

In the present study the effect of the tilt angle on the onset of erosion as well as the effect of a flow on the avalanche angle has been investigated in laminar flow conditions. For flat beds and for different grain diameters, results have been compared to previous experimental results found in the literature and to a simple model of erosion. Results are consistent with a constant critical Shields number $\theta_0 \sim 0.14$ for particle Reynolds number $\mathrm{Re}_d < 1$. For $\mathrm{Re}_d > 1$, θ_0 is found to decrease as Re_d^{-1}. When the cell is tilted, the critical Shields number θ_c is modified, increasing for upward flow and decreasing for downward flow. However the relative increase is at first order independent of the grain diameter and then of Re_d. A solid friction model for one grain on a plane accounts well for the experimental results if a large friction angle $\delta = 67.5°$ is incorporated in the model. This value of the friction is higher than the usual Mohr-Coulomb friction angle ($\approx 30°$) or than the geometric stability angle obtained without friction for tetrahedral packing[40] ($\approx 23.8°$). Results also show that the critical angles β_c for granular avalanches are affected by the intensity of the laminar flow above the immersed beads. The experimental evolution is almost linear with the flow rate and can been described by a model taking into account the forces acting on a layer of material submitted to Coulomb friction with the underlying grains. This model fits the data for a constant thickness of the avalanching layer $h \approx 0.5$ mm, independent of the grain diameters for our submillimetric beads. This value is of the order of the observed flowing layer at threshold.

Above the onset the interface evolves either to periodic triangular ripples for small tilt angles or to vortex ripples for large angles. More details on these dynamical structures will be presented elsewhere.

ACKNOWLEDGMENTS

Gérard Chauvin and Rafaël Pidoux are gratefully acknowledged for their technical help. The authors wish to express their appreciation to the various graduate students that worked on this experiment: Marc Leconte, Jean-François-Régis Aulagnier, Anne Planchette, Sophie Ancel, and Marc Ronet. This work also benefitted from fruitful discussions with Pierre-Yves Lagrée, Daniel Lhuillier, Germain Rousseau, Agnès Paterson, and Richard Whitehouse. This work was supported by the French Ministry of Research by the ACI "Jeunes Chercheurs" No. 2114.

APPENDIX: EVALUATION OF THE VISCOUS SHEAR CLOSE TO THE BED

Gondret *et al.*[29] show that the velocity field in a Hele-Shaw cell of rectangular section $b \times H_w$ writes

$$u(y,z) = \frac{3\bar{U}}{2}\left\{1 - \left(\frac{2y}{b}\right)^2 + \sum_{n=1}^{\infty}(-1)^n \frac{32}{(2n-1)^3\pi^3} \times \frac{\cosh[(2n-1)\pi z/b]}{\cosh[(2n-1)\pi H_w/2b]}\cos[(2n-1)\pi y/b]\right\}.$$

Close to the bed location $z \approx -H_w/2$ the velocity gradient $\partial u/\partial z$ writes

$$\left.\frac{\partial u(y,z)}{\partial z}\right|_{z=-H_w/2} = \frac{48\bar{U}}{\pi^2 b}\left\{\sum_{n=1}^{\infty}\frac{(-1)^{n+1}}{(2n-1)^2}\tanh[(2n-1) \times \pi H_w/2b]\cos[(2n-1)\pi y/b]\right\}.$$

If we now average this gradient across the gap thickness b of the cell, we obtain

$$\dot{\gamma} = \left\langle \left.\frac{\partial u(y,z)}{\partial z}\right|_{z=-H_w/2}\right\rangle_y = \frac{96\bar{U}}{\pi^3 b}\left\{\sum_{n=1}^{\infty}\frac{1}{(2n-1)^3} \times \tanh[(2n-1)\pi H_w/2b]\right\}.$$

For $H_w \gg b$, as $\Sigma_{n=1}^{\infty}(2n-1)^{-3} \approx 1.052$, we finally obtain

$$\dot{\gamma} \approx 3.26\bar{U}/b.$$

[1] K. R. Dyer, *Coastal and Estuarine Sediment Dynamics* (Wiley, New York, 1986).
[2] J. Fredsoe and R. Deigaard, *Mechanics of Coastal Sediment Transport*, Advanced Series on Ocean Engineering, Vol. 3 (World Scientific, Singapore, 1992).
[3] M. P. du Boys, "Etude du régime et action exercée par les eaux sur un lit à fond de graviers indéfiniment affouissable," Ann. Ponts Chaussees **5**, 141 (1879).
[4] E. Meyer-Peter and R. Muller, "Formulas for bed-load transport," Proceedings of the International Association on Hydraulic Research, Third Annual Conference, Stockholm (1948), pp. 39–64.
[5] M. S. Yalin, "An expression for bed load transport," J. Hydraul. Div., Am. Soc. Civ. Eng. **89**, 221 (1963).
[6] M. S. Yalin, *Mechanics of Sediment Transport*, (Pergamon, Oxford, 1972).
[7] R. A. Bagnold, "An approach to the sediment transport problem from general physics," U.S. Geol. Surv. Prof. Pap. **422-I**, 1 (1972).
[8] A. Shields, *Anwendung der Ähnlichkeitsmechanik und der Turbulenzforschung auf die Geschiebebewegung*, Mitteilungen der Precuss. Versuchsanst. f. Wasserbau u. Schiffbau Heft 26 Berlin, (1936).
[9] P. Y. Jullien, *Erosion and Sedimentation* (Cambridge University Press, Cambridge, 1998).
[10] L. C. Van Rijn, *Principles of Sediment Transport in Rivers, Estuaries and Coastal Seas* (Aqua Publications, Amsterdam, The Netherlands, 1993).
[11] N.-S. Cheng, A. W.-K. Law, and S. Y. Lim, "Probability distribution of bed particle instability," Adv. Water Resour. **26**, 427 (2003).
[12] J. W. Lavelle and H. O. Mofjeld, "Do critical stresses for incipient motion and erosion really exist?," J. Hydraul. Div., Am. Soc. Civ. Eng. **113**, 370 (1987).
[13] C. M. White, "The equilibrium of grains on the bed of a stream," Proc. R. Soc. London, Ser. A **174**, 322 (1940).
[14] S. J. White, "Plane bed thresholds of fine grained sediments," Nature (London) **228**, 152 (1970).
[15] P. A. Mantz, "Incipient transport of fine grains and flakes by fluids—Extended Shields diagram," J. Hydraul. Div., Am. Soc. Civ. Eng. **103**, 601 (1977).
[16] M. S. Yalin and E. Karahan, "Inception of sediment transport," J. Hydraul. Div., Am. Soc. Civ. Eng. **105**, 1433 (1979).
[17] M. Pilotti and G. Menduni, "Beginning of sediment transport of incoherent grains in shallow shear flows," J. Hydraul. Res. **39**, 115 (2001).
[18] F. Charru, H. Mouilleron, and O. Eiff, "Erosion and deposition of particles on a bed sheared by a viscous flow," J. Fluid Mech. **519**, 55 (2004).
[19] D. K. Lysne, "Movement of sand in a tunnel," J. Hydraul. Div., Am. Soc. Civ. Eng. **95**, 1835 (1969).
[20] J. R. L. Allen, "Sand waves: a model of origin and internal structures," Sediment. Geol. **26**, 281 (1980).
[21] R. J. S. Whitehouse and J. Hardisty, "Experimental assessment of two

theories for the effect of bedslope on the threshold of bedload transport," Mar. Geol. **79**, 135 (1988).
[22]G. D. R. MiDi, "On dense granular flows," Eur. Phys. J. E **14**, 341 (2004).
[23]J. R. L. Allen, "The avalanching of granular solids on dune and similar slopes," J. Geol. **78**, 326 (1970).
[24]M. A. Carrigy, "Experiments on the angles of repose of granular materials," Sedimentology **14**, 147 (1970).
[25]S. Courrech du Pont, P. Gondret, B. Perrin, and M. Rabaud, "Granular avalanches in Fluids," Phys. Rev. Lett. **90**, 044301 (2003).
[26]J. R. L. Allen, *Sedimentary Structures, Vol. II, Their Character and Physical Basis* (Elsevier, Amsterdam, 1982), pp. 149–159.
[27]S. Courrech du Pont, P. Gondret, B. Perrin, and M. Rabaud, "Wall effects on granular heap stability," Europhys. Lett. **61**, 492 (2003).
[28]G. S. Beavers and D. D. Joseph, "Boundary conditions at a naturally permeable wall," J. Fluid Mech. **30**, 197 (1967).
[29]P. Gondret, N. Rakotomalala, M. Rabaud, D. Salin, and P. Watzky, "Viscous parallel flows in finite aspect ratio Hele-Shaw cell: analytical and numerical results," Phys. Fluids **9**, 1841 (1997).
[30]F. Waleffe, "Exact coherent structures in channel flow," J. Fluid Mech. **435**, 93 (2001).
[31]E. Herbolzheimer, "Stability of the flow during sedimentation in inclined channels," Phys. Fluids **26**, 2043 (1983).
[32]J. M. Buffington and D. R. Montgomery, "A systematic analysis of eight decades of incipient motion studies, with special reference to gravel-bedded rivers," Water Resour. Res. **33**, 1993 (1997).
[33]M. E. O'Neill, "A sphere in contact with a plane wall in a slow linear shear flow," Chem. Eng. Sci. **23**, 1293 (1968).
[34]M. R. King and D. T. Leighton, "Measurement of the inertial lift on a moving sphere in contact with a plane wall in a shear flow," Phys. Fluids **9**, 1248 (1997).
[35]R. Clift, J. R. Grace, and M. E. Weber, *Bubbles, Drops and Particles* (Academic, New York, 1978).
[36]J. D. Iversen and K. R. Rasmussen, "The effect of surface slope on saltation threshold," Sedimentology **41**, 721 (1994).
[37]H. Mouilleron-Arnould, "Instabilités d'un lit granulaire cisaillé par un fluide visqueux," Ph.D. thesis, Université Paul Sabatier, Toulouse, France (2002).
[38]G. P. Krishnan and D. T. Leighton, "Inertial lift on a moving sphere in contact with a plane wall in a shear flow," Phys. Fluids **7**, 2538 (1995); **9**, 2174 (1997).
[39]S. Courrech du Pont, "Avalanches granulaires en milieu fluide," Ph.D. thesis, Université Paris Sud, Orsay, France (2003).
[40]R. Albert, I. Albert, D. Hornbaker, P. Schiffer, and A.-L. Barabási, "Maximum angle of stability in wet and dry spherical granular media," Phys. Rev. E **56**, R6271 (1997).